Non-polar organic compounds in aerosols in a typical city of Eastern China: Size distribution, gas-particle partitioning and tracer for PM$_{2.5}$ source apportionment

Deming Han[1], Qingyan Fu[2], Song Gao[2], Li Li[3], Yingge Ma[3], Liping Qiao[3], Hao Xu[1], Shan Liang[1], Pengfei Cheng[4], Xiaojia Chen[1], Yong Zhou[1], Jian Zhen Yu[5], Jinping Cheng[1]

[1] School of Environmental Science and Engineering, Shanghai Jiao Tong University, Shanghai 200240, China

[2] Shanghai Environmental Monitor Centre, Shanghai 200235, China

[3] State Environmental Protection Key Laboratory of the Cause and Prevention of Urban Air Pollution Complex, Shanghai Academy of Environmental Science, Shanghai 200233, China

[4] School of Chemical and Environmental Engineering, Jiujiang University, Jiujiang 332005, Jiangxi, China

[5] Department of Chemistry, The Hong Kong University of Science and Technology, Hong Kong 999077, China

Correspondence to: Jinping Cheng (jpcheng@sjtu.edu.cn); Li Li (lili@saes.sh.cn)

Abstract:Aerosol-associated non-polar organic compounds (NPOCs), including 15 polycyclic aromatic hydrocarbons (PAHs), 30 n–alkanes, 2 iso–alkanes, 5 hopanes and 5 steranes, were identified and quantified in PM$_{2.5}$ samples using thermal desorption–gas chromatography/mass spectrometry (TD-GC/MS) method. The samples were collected in a typical city of Eastern China. The total concentrations of NPOCs were 31.7–388.7 ng m^{-3}, and n–alkanes were the most abundant species (67.2%). The heavy molecular weight PAHs (4- and 5-ring) contributed 67.88% of the total PAHs, and the middle chain length n–alkanes (C$_{25}$–C$_{34}$) were the most abundant in n-alkanes. PAHs and n-alkanes were majorly distributed in 0.56–1.00 μm fraction. ∑(hopanes+steranes) were associated with the 0.32–1.00 μm fraction. Analysis showed that 83.0% of NPOCs were originated from anthropogenic sources, especially pyrogenic sources such as fossil fuel combustion and biomass burning. The ratio–ratio plots indicated that NPOCs in local area were affected by photochemical degradation and emissions from mixed sources. Gas-particle partitioning model showed that the particle-phase fraction (φ) of light molecular weight NPOCs ranged from 2.4% to 62.5%, while that of heavy NPOCs accounted for more than 90.0%. The data based on single particle phase and the data based on gas-particles phases incorporated with other PM$_{2.5}$ compounds were used as input data for positive matrix factorization (PMF) model, respectively. Eight factors were extracted for both cases: secondary aerosol formation, vehicle exhaust, industrial emission, coal combustion, biomass burning, ship emission, dust and light NPOCs. This study provides new information on the profiles of PM$_{2.5}$-associated NPOCs, size-specific distributions, photodegradation and their gas-particle partitioning. This will help us accurately identify the potential sources of aerosols and then asses the contributions from each source.

1. Introduction

In recent years, severe atmospheric pollution characterized by haze has been occurring in developing countries, affecting visibility, optical radiation and human health (Yadav et al., 2013;Wang et al., 2015;Shen et al., 2015;Sulong et al., 2017). China has experienced numerous severe and long-lasting haze episodes since winter in 2013, which has affected over 600 million local residents and covered a quarter of the country's land area (Huang et al., 2014;Hao and Liu, 2015). In essence, haze episode is caused by the distribution of particle matters with different sizes in atmosphere, leading to decrease in visibility (Xie et al., 2017). Carbonaceous aerosols contain a large amount of particle matters, accounting for 30–50% of $PM_{2.5}$ mass concentrations (Yadav et al., 2013;Wang et al., 2016;Ma et al., 2018). Carbonaceous aerosols have significant influence on environmental and physical processes, including dry/wet deposition, cloud condensation nucleation, and heterogeneous reactions (Feng et al., 2006;Li et al., 2017).

Since carbonaceous aerosols can affect ambient environment significantly, it is crucial to investigate aerosol-associated organic compounds. Because non-polar organic compounds (NPOCs) can provide specific information on the identification of aerosol sources, they are now of special interest to researchers (Rajput and Sarin, 2014;Wang et al., 2016). n-Alkanes, polycyclic aromatic hydrocarbons (PAHs), hopanes and steranes are four typical NPOC species, and are frequently used to apportion sources of ambient particulate matters (Xu et al., 2013;Zhao et al., 2016). n-Alkanes are emitted from natural and anthropogenic activities, including particulate abrasion products from leaf surfaces of vegetation and fossil fuel combustion. Notably, fossil fuel combustion is characterized by the release of C_{22}–C_{25} n-alkanes, while particulate abrasion products from leaf surfaces is characterized by the predominance of $>C_{29}$ odd n-alkanes (Yadav et al., 2013). PAHs are mainly emitted from anthropogenic activities, including biomass burning, coal combustion, fossil fuel combustion and industrial processes (Ma et al., 2011;Zhang et al., 2015). Hopanes and steranes are from unburned fossil fuels and lubricant oils, and they are often found in vehicle exhausts, ship emissions and coal combustion emissions.

PAHs are typical semi-volatile organic compounds, which can partition between gas and particle phases in ambient atmosphere (He and Balasubramanian, 2009; Ma et al., 2011). The gas-particle partitioning behavior of semi-volatile organic compounds can be used in their removal process, which is performed through wet/dry deposition, long-range transport and reaction with atmospheric oxidant. Recently, research has shown that n-alkanes, hopanes and steranes are also semi-volatile and subject to gas-particle partitioning (Xie et al., 2013;Xie et al. 2014;Wang et al., 2016). Furthermore, lighter, more volatile compounds show larger partitioning tendency. Additionally, another crucial factor affecting particle-bound concentrations of NPOCs is their aerodynamic diameter (Wang et al., 2009). The size-specific

distributions of compounds are dependent on their physical-chemical properties, gas-particle partitioning and photodegradation (Okonski et al., 2014;Chen et al., 2016b). Thus, characterization of the size-specific distribution of NPOCs is crucial for understanding their formation, assessing their possible environmental fate and offering proper management (Kleeman et al., 2008;Wang et al., 2009). Although several studies have focused on the size distribution of PAHs, much less attention has been given to other NPOC species (Hien et al., 2007;Wang et al., 2009).

NPOCs are typically assumed to be stable and nonreactive (Feng et al., 2006;Ma et al., 2011). However, recent research has shown that NPOCs can be oxidized by $\cdot$OH radicals, $RO_2\cdot$ radicals and O_3 over atmospherically relevant time scales (Xie et al., 2013;Wang et al., 2016). PAHs, n-alkanes, hopanes and steranes can undergo photochemical oxidation, increasing the production of secondary organic aerosol (Robinson et al., 2006;May et al., 2012). For example, PAHs can react with $\cdot$OH radicals, and through adding carbonyl groups to the carbon skeleton, the free ends of C-C scission products remain tethered together, which prevents fragmentation and leads to more functional groups on the single product (May et al., 2012). Hence, the low-volatility species which can condense into particle phase are formed, and subsequently undergo oligomerization reactions following condensation.

To develop strategies for controlling atmospheric pollution caused by particulate matter, receptor-based models (e.g., positive matrix factorization, PMF) have been widely applied to quantitatively apportion sources of particulate matter (Wang et al., 2009;Li et al., 2016;Huang et al., 2017). However, the output factors of receptor model are not necessarily emission sources, because there exist some atmospheric processes like photodegradation or gas-particle partitioning. Considering the gas-particle partitioning of NPOCs, Xie et al. (2013) adopted both gaseous and particulate NPOCs in PMF model and successfully extracted seven factors. More recently, Wang et al. (2016) used data of NPOCs combined with those of organic/elemental compounds (OC/EC), inorganic compounds and elemental compounds as input for PMF model, and they found that total (gas + particle) bound concentrations enabled more reasonable source profiles than single particle phase.

In this paper, we conducted a comprehensive study on $PM_{2.5}$-associated NPOCs in a typical city of Eastern China. Specifically, we: (1) quantified the concentrations of NPOCs (n–alkanes, PAHs, hopanes and steranes) through thermal desorption–gas chromatography/mass spectrometry (TD–GC/MS) method; (2) determined the size-specific distributions of NPOCs from 0.01 to 18 μm; (3) analyzed the degradation of NPOCs; (4) explored the gas-particle partitioning of NPOCs and assessed its effects on $PM_{2.5}$ source apportionment.

2. Materials and methods

2.1 Sampling sites and sample collection

Jiujiang city is located in $113^o57'$–$116^o53'$ E and $28^o47'$–$30^o06'$ N with elevation of 32 m in Jiangxi Province of Eastern China. It is characterized by a subtropical monsoon climate. Jiujiang is the second largest city in Jiangxi Province, with approximately 4.83 million resident population and over 700 thousand motor vehicles in 2015. Preliminary statistics indicate that the gross industrial standard coal consumption in Jiujiang amounted to 7.80 million tons in 2015. In Jiujiang, petrochemical industry, which can process approximately five million tons of crude oil per year, is located at the northeast part of the city and in upwind direction. In addition, Mount Lu (elevation of 1474 m), located at the south of Jiujiang, blocks the transport of air masses from Northern China Plain region to southern area, leading to the accumulation of particulate matters in the city area, especially in winter seasons.

Five $PM_{2.5}$ sampling sites were selected for routine air quality measurements in Jiujiang city (Table 1), including Shihua (SH), Xiyuan (XY), Shili (SL), Wuqierqi (WQ) and Jiujiangxian (JJ). All $PM_{2.5}$ filter samples were collected using medial-volume air samplers (YH-5, Qingdao, China), at a flow rate of 100 L min^{-1}. Particles were collected on quartz fiber filters (GE Whatman, 1851-090, England, UK) with a diameter of 90 mm, each for a duration of 23 h. Prior to use, these filters were prebaked at 550 ^{o}C for 4 h to eliminate residual organic compounds. $PM_{2.5}$ sampling at these five sites were performed synchronously for five continuous days per month from Sep. to Dec. 2016, in addition to the extensive sampling period (Dec. 1–16). A total of 137 $PM_{2.5}$ valid samples were collected, as 18 samples were invalid or missing due to the bad weather or power problems during sampling period.

Table 1. Detailed description of the six sampling sites in this study

Site	Type	Surrounding area	Height	Main pollutants	Sampling time
SH	Residential area	1.7 km to petrochemical industry; 600 m to traffic road	~12 m	Petrochemical industry	Sep. 9-13; Oct. 11-15; Nov. 10-14; Dec. 1-16
XY	Urban area	500 m to traffic road; 1 km to wharf	~23 m	Vehicle; ship	Sep. 9-13; Oct. 11-15; Nov. 10-14; Dec. 1-16
SL	Urban center	500 m to traffic road	~20 m	vehicle	Sep. 9-13; Oct. 11-15; Nov. 10-14; Dec. 1-16
WQ	Suburban area	1.3 km to the city center	~17 m	vehicle	Sep. 9-13; Oct. 11-15; Nov. 10-14; Dec. 1-16
JJ	Industrial area	Located in industrial area; 500 m to highway	~20 m	Industry emission	Sep. 9-13; Oct. 11-15; Nov. 10-14; Dec. 1-16
EM	Urban area	500 m to traffic road	~20 m	vehicle	Dec. 1-16

The sampling site of size–specific aerosols was located at a five–story building of Jiujiang Environmental Monitor Station (EM site). Airborne particle samples were collected for 23 h using a Nano–Micro–orifice Uniform Deposition

108   Impactor (MOUDI) sampler (Model 122R, MSP Cor, USA), at air flow rate of 30 L/min. Detailed instrument operation,

109   quality assurance and control method can be found in our previous work (Chen et al., 2016b;Han et al., 2018). Briefly,

110   this sampler can collect particles within 13 size fractions: 0.01–0.018, 0.018–0.032, 0.032–0.056, 0.056–0.1, 0.1–0.18,

111   0.18–0.32, 0.32–0.56, 0.56–1.0, 1.0–1.8, 1.8–3.1, 3.1–6.2, 6.2–9.9, 9.9–18 μm. Prior to sampling, each filter tray was

112   washed with distilled water and ethanol. Two kinds of quartz fiber filters of diameters of 47 and 90 mm were used to

113   collect particles with diameter of 0.056-18.0 and 0.010-0.056 μm, respectively. All the filters were prebaked at 550 ^{o}C for

114   4 h, wrapped in aluminum foil and then sealed in clean polyethylene bags. Leak and flow tests were conducted according

115   to manufacturer's instructions: leak test was done with a duration of 60 s with leak rate < 10 Pa/s at initial pressure of

116   55±5 kPa. The mass concentrations of particle matters were determined by subtracting the filter weight before and after

117   sampling. A well calibrated digital balance within a precision of 0.01 mg (Sartorius SE2, Germany) was used. The

118   collected particle samples were stored at controlled temperature (–20 ^{o}C) and relative humidity until analysis.
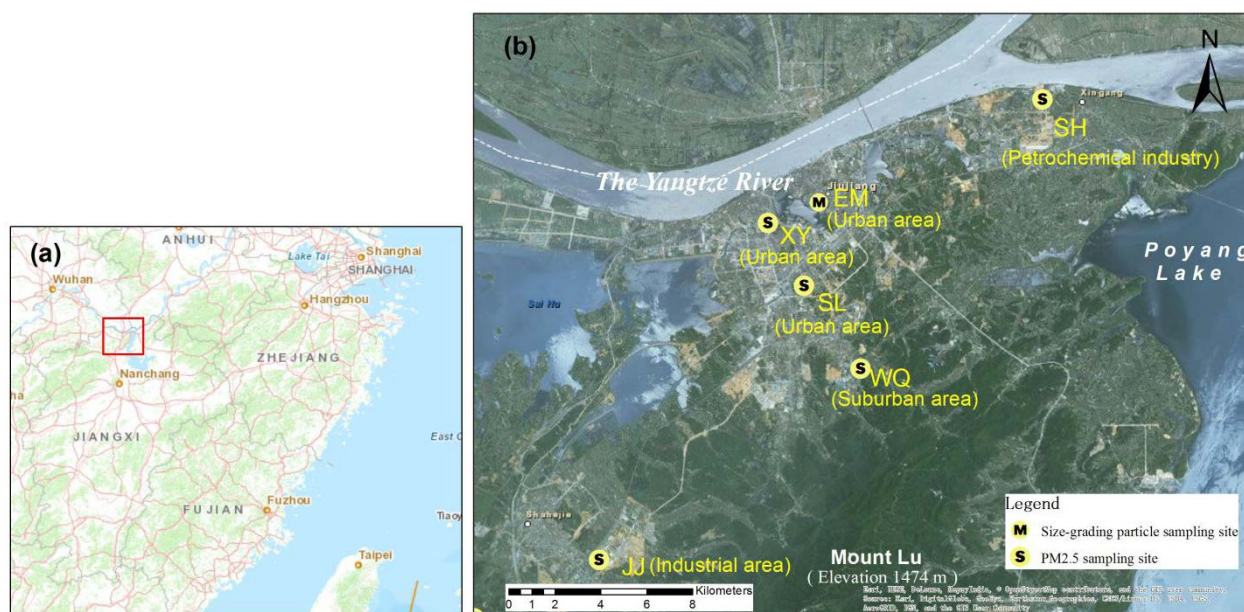
119

120   **Fig. 1.** Location of aerosol sampling sites in Jiujiang City, Eastern China

121   **2.2 Analysis of aerosol samples using TD–GC/MS**

122   Fifty-seven NPOC species (Table 2) were identified by using an in-injection port thermal desorption union (TDU,

123   Shimadzu, Japan), coupled with gas chromatography/mass spectrometer (GC/MS, QP2010 Plus, Shimadzu, Japan).

124   Compared with traditional solvent extraction method, TD–GC/MS method (Ho and Yu, 2004;Ho et al., 2008) has

125   advantages such as solvent and sample filtration, labor saving, and less contamination from solvent impurities. A filter

126   aliquot (1 cm^2) from quartz fiber was cut into small pieces on a clean glass dish, and then they were inserted into the TD

127   tubes (CAMSCO, USA). Both sides of the samples were surrounded with pre-baked, silane-treated glass-wool plugs, to

enhance the cryofocusing of the analytes and prevent heavy and polar compounds from entering the GC column. The internal standards of n–tetracosane d_{50} (n–$C_{24}D_{50}$), naphthalene–d_8, acpnaehthene–d_{10}, phenanthrene–d_{10}, and chrysene–d_{12} were spiked into each sample, through a pipette with a long thin tip. This was done to account for the loss of components from sample filters associated with the instrument instability due to changes in laboratory environmental conditions. After the evaporating of solvent from internal standard was conducted via air drying for several seconds, the TD tubes were capped and put into a sampler holder.

The sample processing time in TD tube was set to 45 min, and the TD tube was electronically cooled to −10 $^{\circ}$C. The desorption and interface temperatures were set to 295 and 280 $^{\circ}$C, respectively. Helium (99.999%) was used as carrier gas for the thermally desorbed organic compounds, with gas flow rate of 1.12 mL/min. GC was used under splitless injection mode, and the initial oven temperature was set to 40 $^{\circ}$C with an isothermal hold time of 5 min. Stepwise programmed linear temperature ramping included 10 $^{\circ}$C/min to 120 $^{\circ}$C (held for 2 min), and then 20 $^{\circ}$C/min to 300 $^{\circ}$C (kept for 20 min). A Rtx–5MS capillary column (Restek, USA, L × I.D. 30 m × 0.25 mm, df 0.25 μm) was used to separate desorbed organic compounds. The MS was operated in scan mode with mass range was m/z 50–500, and scanned at 0.5 s/scan (Ho et al., 2008;Yadav et al., 2013). The ion was produced from electronic impact ionization (EI) at 70 eV, and then was separated by high performance quadrupole mass filter. Species identification was achieved via comparing the mass spectra and retention times of the chromatographic peak with the corresponding authentic standards.

Table 2. Abbreviation, P^{o}_{L} and ΔH_0 information for individual NPOCs

Species	Abb.	P^{o}_{L} [a]	ΔH_0 [b]	Species	Abb.	P^{o}_{L}	ΔH_0
PAHs				**n–Alkanes**			
Fluorene	FLO	1.10E–01	84.9	n–Undecane	$C_{11}H_{24}$	/	/
Phenanthrene	PHE	2.57E–02	88.9	n–Dodecane	$C_{12}H_{26}$	/	/
Anthracene	ANT	1.21E–03	99.7	n–Tridecane	$C_{13}H_{28}$	/	/
Fluoranthene	FLU	1.60E–03	98.3	n–Tetradecane	$C_{14}H_{30}$	/	/
Pyrene	PYR	7.60E–04	97.9	n–Pentadecane	$C_{15}H_{32}$	/	/
Benz[a]anthracene	BaA	3.45E–05	108	n–Hexadecane	$C_{16}H_{34}$	/	/
Chrysene	CHR	1.36E–06	118.8	n–Heptadecane	$C_{17}H_{36}$	/	/
Benzo[b]fluoranthene	BbF	1.00E–06	119.2	n–Octadecane	$C_{18}H_{38}$	/	/
Benzo[j+k]fluoranthene	BkF	4.66E–06	113	n–Nonadecane	$C_{19}H_{40}$	/	/
Benzo[a]fluoranthene	BaF	4.66E–05	113	n–Eicosane	$C_{20}H_{42}$	/	/
Benzo[e]pyrene	BeP	7.89E–07	117.9	n–Heneicosane	$C_{21}H_{44}$	/	/
Indeno[1,2,3-cd]pyrene	IcdP	1.42E–06	124	n–Docosane	$C_{22}H_{46}$	3.24E–03	115
Dibenz[a,h]+[a,c]anthracene	DahA	4.93E–09	134.1	n–Tricosane	$C_{23}H_{48}$	1.22E–03	120
Benzo[ghi]perylene	BghiP	1.01E–08	129.9	n–Tetracosane	$C_{24}H_{50}$	4.66E–04	124
Coronene	COR	3.56E–10	143.2	n–Pentacosane	$C_{25}H_{52}$	1.72E–04	129
iso–Alkane				n–Hexacosane	$C_{26}H_{54}$	6.59E–05	133
Pristane	$C_{19}H_{40}$	/ [c]	/	n–Heptacosane	$C_{27}H_{56}$	2.53E–05	137

Phytane	$C_{20}H_{42}$	/	/	n–Octacosane	$C_{28}H_{58}$	9.42E–06	142
Hopane				n–Nonacosane	$C_{29}H_{60}$	3.55E–06	146
αβ–Nnorhopane	C_{29}–αβ–NOR–H	2.74E–06	126	n–Triacontane	$C_{30}H_{62}$	1.32E–06	151
αβ–Hopane	C_{30}–αβ–H	1.01E–06	130	n–Hentriacontane	$C_{31}H_{64}$	4.96E–07	155
αβ–22R–Homohopane	C_{31}—αβ–R	3.85E–07	134	n–Dotriacontane	$C_{32}H_{66}$	1.93E–07	160
ab 22S–Homohopane	C_{31}—αβ–S	3.85E–07	134	n–Tritriacontane	$C_{33}H_{68}$	7.09E–08	164
22,29,30–Trisnorhopane	Tm	1.93E–05	117	n–Tetratriacontane	$C_{34}H_{70}$	2.63E–08	169
Sterane				n–Pentatriacontane	$C_{35}H_{72}$	1.00E–08	173
ααα–20R Cholestane	ααα–20R–C	2.03E–05	121	n–Hexatriacontane	$C_{36}H_{74}$	3.75E–09	177
αββ–20R Cholestane	αββ–20R–C	/	/	n–Hepatriacontane	$C_{37}H_{76}$	1.42E–09	182
αββ–20R24S–Methylcholestane	αββ–20R–MEC	7.60E–06	125	n–Octatriacontane	$C_{38}H_{78}$	5.37E–10	186
aaa 20R24R–Ethylcholestane	ααα–20R–EC	/	/	n–Nonatriacontane	$C_{39}H_{80}$	2.03E–10	191
αββ–20R24R–Ethylcholestane	αββ–20R–EC	2.84E–06	130	n–Tetracontane	$C_{40}H_{82}$	7.60E–11	195

145   [a]: pure compound vapor pressure, unit of Pa at 298 K, cited from And and Hanshaw, 2004, Xie et al., 2013;

146   [b]: vaporization enthalpy, unit of (KJ mol^{-1}) at 298 K, cited from Xie et al., 2013, Wang et al., 2016;

147   [c]: "/" means lack of related data.

148 **2.3 Determination of OC/EC and other constituents**

149 OC and EC were analyzed (a round punch of 0.538 cm^2) using the thermal–optical– transmittance (TOT) method

150 (NIOSH protocol, Desert Research Institute, USA). The instrument included a temperature- and atmosphere-controlled

151 oven and a laser of 680 nm wavelength to generate an operational EC/OC split. The instrument was heated stepwise from

152 start to 250 ^{o}C (60 s), 500 ^{o}C (60 s), 650 ^{o}C (60 s) and finally 850 ^{o}C (90 s) in the helium atmosphere for OC

153 volatilization, and from start to 550 ^{o}C (45 s), 650 ^{o}C (60 s), 750 ^{o}C (60 s) and finally 850 ^{o}C (80 s) in the helium

154 atmosphere containing 2% oxygen for EC oxidation.

155 Elemental compositions, including Na, K, Ca, Mg, P, Fe, Ti, Al, Pb, Cu and Zn, were determined by energy dispersive

156 X-ray fluorescence (ED-XRF) spectrometry (Epsilon 5, Netherlands). Water soluble inorganic ions, including cations

157 (Na^+, K^+, Mg^{2+}, Ca^{2+}, NH_4^+) and anions (Cl^-, SO_4^{2-} and NO_3^-, NO_2^-), were detected by ion chromatography (IC, ISC-90,

158 Dionex, USA).

159 **2.4 Quality assurance and quality control**

160 Prior to sampling in each site, the five PM$_{2.5}$ samplers were calibrated by environmental monitor station. PM$_{2.5}$ samplers

161 were placed on the building rooftop of Jiujiang Environmental Monitor Station, each two within distance of <3 m. Field

162 blanks were collected by keeping blank filters in the sampler for the same duration at sampling site. Additionally, both

163 transport and laboratory blank filters were analyzed, and all the data reported in this study were corrected according to

164 the results.

 The NPOCs standards used were National Institute of Standards and Technology (NIST, USA) Standard Reference

166 Materials (SRM), including SRM 2260A, SRM 1494 and SRM 2266 for 15 PAHs, 30 n-alkanes and 10 hopanes/steranes,

167 respectively. Six–point calibration curves of NPOCs were constructed through adopting different calibration

168 solutions, namely 0, 0.05, 0.25, 0.50, 1.0 and 2.0 μg L^{-1} for PAHs, hopanes and steranes, while 0, 0.10, 1.0, 5.0, 10.0

169 and 20.0 μg L^{-1} for n–alkanes, to the field blank filters and loaded into TD tubes. The same concentration of internal

170 standards were used for each level of calibration solution. Ratios of the average peak area values 'A' for represented

171 samples 'S' to the corresponding internal standard 'IS', namely AS/AIS; and ratios of average concentration 'C' for

172 represented samples to the corresponding internal standard (CS/CIS), were generated via using Shimadzu software

173 with the slope of the curve being the RRF (relative response factor). The calibration curves for most target

174 compounds were highly linear (r^2>0.99), demonstrating the consistency and reproducibility of this method. The

175 standard deviation (S) was calculated by using seven replicates of the second lowest standard solution, and the

176 method detection limit (MDL, MDL =3.143×S) was determined at the 99% confidence level.

177 Recovery experiment were conducted to improve the desorption of targeted compounds from filters and

178 experimental detection. The analytical recovery was calculated via spiking a known amount of the solution to blank

179 filter, and most compounds were recovered with recovery efficiency >90% except for several light molecule weight

180 species. The accuracy of the method was evaluated by reproducibility of the standard and selected samples

181 ascertained by processing in quintuplicate, and results suggest the analytical precision was better than 5%.

182 **2.5 Diagnostic parameters and isomeric ratios**

183 Different diagnostic parameters were adopted in this study to explore natural and anthropogenic contributions. The

184 parameters include carbon preference index (CPI), the carbon number of the most abundant n–alkane (C_{max}),

185 contributions from natural wax n–alkanes (WNA%) and petrogenic n–alkanes (PNA%), higher plant n–alkane average

186 chain length (ACL), and molecular diagnostic ratios (MDRs) for PAHs (Yadav et al., 2013;Zhao et al., 2016).

187 (1) CPI is defined as the ratio of the total concentration of odd n–alkanes to that of even n–alkanes (Eq. (1)). It reflects

188 the comparison between natural and anthropogenic contributions.

189
$$CPI = \frac{\sum_{i=11}^{39} C_i}{\sum_{j=12}^{40} C_j} \qquad (1)$$

190 where i and j represent odd and even carbon numbers, respectively, and C represent the concentrations of carbon n–

191 alkanes.

192 (2) WNA% is calculated as Eq. (2). Note that negative value of $[C_i – (C_{i–1} + C_{i+1})/2]$ was replaced by zero.

193 $$\text{WNA\%} = \frac{\sum \text{WNA}_{C_n}}{\sum \text{NA}_{C_n}} = \frac{\sum_{i=11}^{39} \left[C_i - (C_{i-1} + C_{i+1})/2 \right]}{\sum_{n=11}^{40} C_n} \quad (2)$$

194 (3) Aerosol–associated n–alkanes can originate from plant wax or petroleum combustion, and the percentage of

195 petrogenic n–alkanes (PNA%) can be calculated as:

196 $\text{PNA\%} = 100\% - \text{WNA\%} \quad (3)$

197 (4) C_{max} represents the carbon number of the most abundant n–alkane, and it is regarded as the most important indicator

198 of biogenic inputs. In general, $C_{max} = 31$ indicates effects from leaf abrasion products, whereas $C_{max} = 29$ implies effects

199 from road dust, as well as vehicle and industrial emissions.

200 (5) ACL can indicate emissions of n–alkanes from plants which are related to temperature and humidity. It is defined as

201 counted carbon atoms per carbon molecule, depending on the odd n–alkanes from higher plant. ACL can be estimated

202 through Eq. (4) as follows:

203 $$\text{ACL} = \frac{23 \cdot C_{23} + 25 \cdot C_{25} + \cdots + 39 \cdot C_{39}}{C_{23} + C_{25} + \cdots + C_{39}} \quad (4)$$

204 (6) MDRs for PAHs source apportionment include ANT/PHE ratio, PYR/FLU ratio, IcdP/BghiP ratios (namely,

205 ANT/(ANT+PHE) ratio and FLU/(FLU+PYR) ratio), and IcdP/(IcdP+BghiP). If ANT/(ANT+PHE) < 0.1, petroleum

206 origins are suggested; if the ratio > 0.1 pyrogenic sources are indicated. If FLU/(FLU+PYR) < 0.4, petroleum sources are

207 suggested; if the ratio > 0.4, pyrogenic sources are indicated (Kuang et al., 2011;Chen et al., 2016a). Note that the ratio

208 ranging from 0.4 to 0.5 also suggests fuel combustion. If 0.2 < IcdP/(IcdP+BghiP) < 0.5, fuel combustion is suggested; if

209 the ratio > 0.5, grass, wood and coal combustion should have contributed to particulate matters (Chen et al., 2016a).

210 **2.6 Gas-particle partitioning model**

211 Gas-particle partitioning is an important mechanism that affects the fate and transport of NPOCs (Pankow, 1994;Kim et

212 al., 2011). To understand the partitioning behavior of NPOCs, we evaluated the distribution of NPOCs between gas and

213 particle phases in the atmosphere. The gas-particle coefficient K_p (m³ μg⁻¹) for each compound species was calculated

214 using the following equations:

215 $$K_p = \frac{F/PM}{A} = \frac{R \cdot T}{10^6 \cdot MW_{OM} \cdot \xi_{OM} \cdot P_L^o} \quad (5)$$

216 $$P_L^o = P_{L,0}^o \cdot \exp\left[\frac{\Delta H_0}{R} \left(\frac{1}{298} - \frac{1}{T} \right) \right] \quad (6)$$

217 where F and A represent the concentrations of NPOC in gas and particle phases (ng m⁻³), respectively; PM is the

218 measured mass concentration of particulate matter, *i.e.*, PM$_{2.5}$ in this study (μg m⁻³); R is the ideal gas constant (8.314 m³

219 Pa^{-1} K^{-1} mol^{-1}); T is the ambient temperature (K); MW$_{OM}$ is the mean molecular weight (g mol^{-1}), and is 200 g mol^{-1} in

220 this study (Xie et al., 2013); ξ_{OM} is the activity coefficient of each compound in the absorbing phase and assumed to be

221 unity in this calculation (Xie et al., 2013); P^o_L and P$^o_{L,0}$ are subcooled vapor pressures at T and 298 K, respectively (Pa);

222 ΔH_0 is vaporization enthalpy of the liquid at 298.15 K. The measured P^o_L and ΔH_0 were extracted from previous

223 literatures (And and Hanshaw, 2004;Wang et al., 2016).

224 The total concentration (S) of each NPOC in gas and particle phases was calculated as Eq. (7):

225 $$S = F + A = (1 + \frac{10^6 \cdot MW_{OM} \cdot \xi_{OM} \cdot P^o_L}{R \cdot T \cdot PM}) \times F \quad (7)$$

226 Also, Jungle–Pankow model was further used to investigate gas-particle partitioning. In this model, the ratio (φ) of the

227 concentration of NPOC species in particle phase to the total NPOC concentration was calculated:

228 $$\varphi = \frac{C_p}{C_p + C_g} = \frac{c \cdot \theta}{c \cdot \theta + P^o_L} \quad (8)$$

229 $$\log Kp = \log \frac{c \cdot \theta}{PM} - \log P^o_L \quad (9)$$

230 where θ represents particle surface area per unit volume of air (cm^2 cm^{-3}) and c is a constant which depends on

231 thermodynamics of the adsorption process, molecular weight, and surface properties (Pa cm^{-1}). In this study, c = 17.2 Pa

232 cm^{-1}, and θ is 1.1×10^{-5}, 1.5×10^{-6} and 4.2×10^{-7} (cm^2 cm^{-3}) for urban area, rural area and background, respectively.

233 **3. Results and discussion**

234 **3.1 Abundance of PM2.5 and NPOCs**

235 The statistical summary and the abundance of measured PM$_{2.5}$ and NPOC species are shown in Fig.2 and Table S1. The

236 average PM$_{2.5}$ concentration in all sampling sites was 79.3±37.7 μg m^{-3}. The average OC and EC concentrations were

237 13.8±6.9 and 6.3±2.2 μg m^{-3}, respectively. Organic matter (OM) was the most abundant component in PM$_{2.5}$, accounting

238 for 18.8–27.8% of the total mass in this study, which was estimated to be 1.4 times of OC concentration (Feng et al.,

239 2006;Huang et al., 2014). Following OM, NO$_3^-$, SO$_4^{2-}$ and NH$_4^+$ were also abundant, accounting for 19.9–22.6%, 16.4–

240 18.1% and 10.4–13.7% of PM$_{2.5}$, respectively.

241 Fifty-seven NPOCs were identified in this study (Table 3), including 30 n-alkanes, 2 iso-alkanes, 15 PAHs, 5 hopanes

242 and 5 steranes. Their total concentrations ranged from 31.7 to 388.7 ng m^{-3} (an average of 155.9±55.4 ng m^{-3}), accounting

243 for 0.4–2.4% of OM. This was consistent with the measurement results of NPOCs in Pearl River Delta (PRD) (Wang et

244 al., 2016) and South China Sea (Zhao et al., 2016) in China, with percentages of 0.1–4.2% and 0.8–1.7%, respectively.

245 n-Alkanes were the most abundant NPOCs, with concentration of 105.3±55.1 ng m^{-3}, accounting for 67.2% of NPOC

concentration. PAHs was the second most abundant species, averagely accounting for 29.2% of NPOC concentration. Hopanes and steranes were minor constituents, with average concentrations of 3.6±3.0 and 1.8±1.3 ng m^{-3}, respectively. The level of n-alkanes in Jiujiang was comparable to those in Shanghai (Feng et al., 2006) and Hong Kong (Li et al., 2013), but a bit higher than those in Guangzhou (Xu et al., 2013), British Columbia (Ding et al., 2009) and South China Sea (Zhao et al., 2016). However, concentrations of PAHs in Beijing and Delhi were 1.7 and 8.2 times higher than that in Jiujiang, respectively.

Table 3. Comparison of NPOC concentrations between Jiujiang City and other areas (ng m^{-3})

	n-Alkane [a]	PAHs [b]	Hopane [b]	Sterane [b]	Time	Reference
Jiujiang, China	105.3±55.1 (16.3–305.0); C_{11}–C_{40}	45.3±17.6 (12.3–96.5); 15	3.6±3.0 (0.6–16.4); 5	1.8±1.3 (0.3–7.0); 5	2016.9–12	This study
Shanghai, China	32.9–341.9; C_{17}–C_{36}	7.8–151.1; 15	/	/	2002–2003	Feng et al., 2006
Beijing, China	163.0±193.5; C_{20}–C_{35}	78.7±115.4; 16	6.9±6.6; 4	/	2004	Feng et al., 2006
Guangzhou, China	48.1±20.8; C_{19}–C_{40}	19.0±17.5; 18	/	/	2010.11	Xu et al., 2013
South China Sea	15.7–124.2; C_{15}–C_{38}	3.4–127.9; 22	0.4–19.6; 8	0.4–3.5; 6	2013.9–10	Zhao et al., 2016
Hong Kong, China	97.9; C_{29}–C_{33}	13.5; 15	21.5			Li et al., 2013
PRD [c], China	1.6–436(64); C_{22}–C_{38}	0.1–74(14.2); 17	0.3–21(2.3);10	0.01–4.1(3.4);5	2011–2012	Wang et al., 2016
British Columbia Canada	4.89–74.38(15.58); C_{11}–C_{40}	1.01–41.7 (10.82); 16	/	/	2005.12–2007.2	Ding et al., 2009
Delhi, India	425±343; C_{12}–C_{35}	373±197; 17	/	/	2006–2009	Yadav et al., 2013

[a]: mean concentration (concentration range); species;

[b]: mean concentration (concentration range); number of species;

[c]: including four cities in PRD: Guangzhou, Dongguang, Nanhai and Nansha.
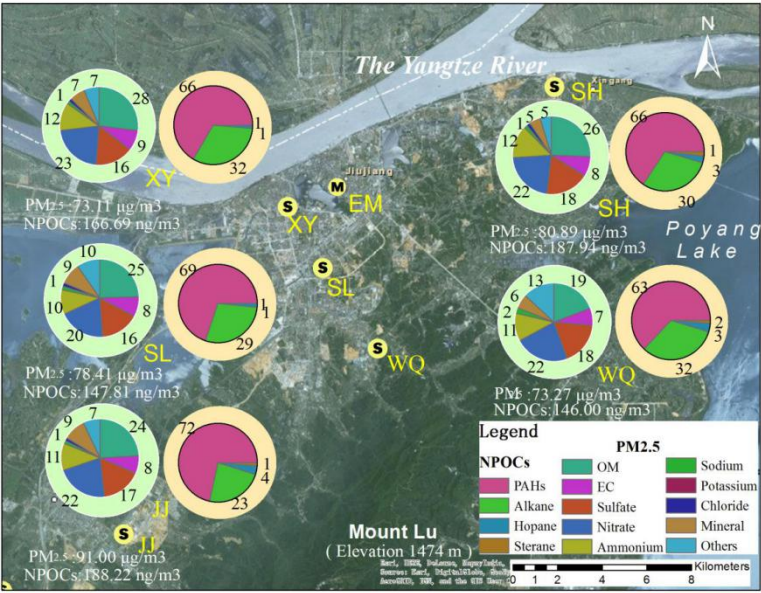
Fig. 2. Spatial distributions of NPOCs and PM$_{2.5}$ in Jiujiang city

258   **3.1.1 PAHs**

259   PAHs are ubiquitous pollutants of the environment. They are originated from natural and anthropogenic sources such as

260   biomass burning, vehicle exhausts, residential heating, waste incineration and industrial emissions. It is well established

261   that the atmospheric concentration and lifetime of PAHs are highly dependent on their gas-particle partitioning behavior,

262   transformation and degradation. The $PM_{2.5}$-associated PAHs were shown in Fig. 3a. Their individual concentrations

263   varied between 0.4 and 5.7 ng m^{-3}. BbF (5.7 ng m^{-3}) was the most abundant PAH species, followed by BaA (5.6 ng m^{-3})

264   and BaP (4.2 ng m^{-3}), together accounting for 34.2% of all PAHs, this was consistent with some previous studies in

265   Guangzhou (Xu et al., 2013). Because of the strong carcinogenic effect of BaP, special attention should be given to it, the

266   level of which was also higher than that indicated by the air quality guideline of WHO (1 ng m^{-3}).

267   Because of the vapor pressure dependent partitioning, 2- and 7-ring PAHs distributed majored in gas and particle phases,

268   respectively. However, PAHs with 3–6 rings appeared in both gas and particle phases through gas-particle partitioning.

269   The total percent contribution of 4- and 5-ring PAHs was 67.9% in this study. FLU–PYR–CHR and BaA–BaP congeners

270   of the 4-ring PAHs often indicate diesel vehicle and biomass combustion (Yadav et al., 2013), respectively, and 5-ring

271   BkF is considered as marker of vehicle tracer. This suggests biomass burning and fossil fuel combustion have mixed

272   effects on local pollution.

273   MDRs of atmospheric PAHs with similar molecular weight have been widely used as a useful tool for aerosol source

274   identification. In this study, the ANT/(PHE+ANT) ratios varied in 0.28–0.68 (mean of 0.48), confirming a strong

275   influence from pyrogenic emissions (Xu et al., 2013;Yadav et al., 2013). Most samples had FLU/(FLU+PYR) ratios of

276   0.36–0.58, implying combined effects of pyrogenic emission and combustion of fuel, grass, wood and coal (Kuang et al.,

277   2011;Chen et al., 2016a). The average IcdP/(IcdP+BghiP) ratio was 0.57, and in most cases the ratio > 0.50, suggesting

278   significant impacts from the combustion of grass, wood and coal. Despite MDRs have been consistently used for source

279   identification, it remains a rather rough method and contradictions may occur. Therefore, more samples should be

280   collected to achieve better results.

281
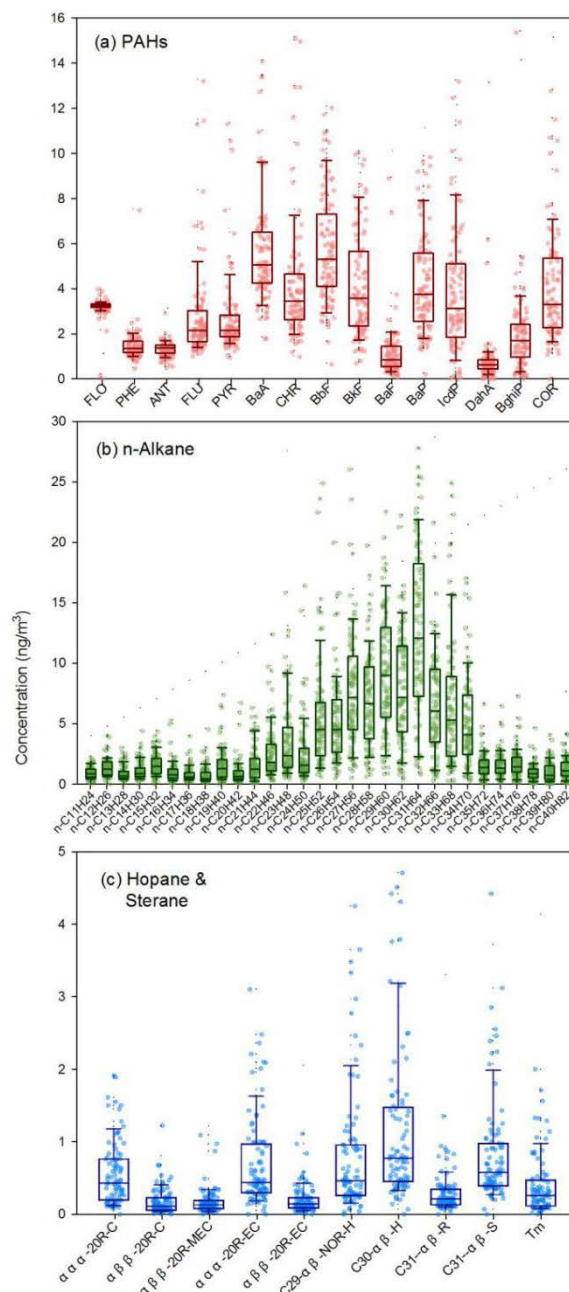
282   **Fig.3.** Concentration profiles of NPOCs

283   **3.1.2 n-Alkanes**

284   Unique signatures of n-alkanes have been shown for different sources, including vehicle exhausts, tire-wear particles,

285   road dust, cooking oil, cigarette smoke and particulate abrasion products from leaf epicuticular waxes (Rogge et al.,

286   1994;Ma et al., 2011;Yadav et al., 2013;Zhang et al., 2015). A bimodal distribution of chain lengths of n-alkanes with

287   peaks at C_{20}–C_{22} and C_{24}–C_{27} implies vehicle exhaust sources (Zhang et al., 2015). However, a unimodal distribution of

288   chain lengths of >C_{30} n–alkanes (peak at C_{37}) represents tire-wear particle sources. The distribution pattern characterized

289   by large proportion of C_{27}–C_{33} odd n–alkanes suggests vegetation sources.

290 Our analysis showed that the middle-chain-length n-alkanes (C_{25}–C_{34}) were the most abundant (Fig. 3b), accounting for

291 72.3% of the total measured n-alkanes. Feng et al. (2006) and Xu et al. (2013) reported similar findings that C_{27}–C_{29}

292 n-alkanes dominated the distribution of n-alkanes in three metropolitan cities of China (Beijing, Shanghai, Guangzhou).

293 In addition, a predominance of odd carbon numbered congeners (C_{25}, C_{27}, C_{29}, C_{31} and C_{33}) was found, with $C_{max} = 31$ in

294 most cases and $C_{max} = 29$ in a few cases (Fig. 3b). The C_{max} value in this study suggests that road dust, cigarette smoke

295 and tire-wear abrasion products have all contributed to n-alkanes in Jiujiang city. However, no obvious odd/even carbon

296 preference was observed for either C_{11}–C_{14} nor C_{35}–C_{40} n–alkanes.

297 Plant wax n-alkanes exhibit strong odd/even carbon number predominance, while n-alkanes from fossil fuel combustion

298 do not (Feng et al., 2006). Thus, biogenic n-alkanes should have CPI values greater than unity, whereas anthropogenic

299 n-alkanes should have CPI values close to unity. Furthermore, CPI < 2 is a typical characteristic of urban environment,

300 suggesting major contribution from petrogenic sources, e.g., vehicle exhausts and industrial emissions. The CPI values

301 were 1.00–1.79 (average of 1.29) in this study, implying strong contributions from petrochemical sources, diesel residues

302 and gasoline emissions. Ding et al. (2009) reported a mean CPI value of 1.5 in central British Columbia of Canada, and

303 Xu et al. (2013) reported CPI values of 1.2–1.7 (mean of 1.4) in Guangzhou of China. The mean contribution of plant

304 wax n-alkanes to the total n-alkanes (WNA%) was 17.00±4.41%, ranging from 7.94% to 31.31%. PNA% provides a

305 direct insight into n-alkanes from petrogenic sources. In this study, PNA% was 83±4.41%, implying that 83% of

306 n-alkanes were originated from anthropogenic sources. The ACL value varied from 27.45 to 30.95. This small

307 fluctuations may suggest that emissions were similar at different sites, which was consistent with the result of Delhi in

308 India (Yadav et al., 2013).

309 **3.1.3 Hopanes and steranes**

310 Hopanes and steranes are usually found in crude oil and engine oil, subsequently in vehicle exhausts from unburned

311 lubricating oil residues. They are regarded as markers of fossil fuel combustion. The concentration profile of hopanes and

312 alkanes was shown in Fig. 3c. Their total concentrations ranged from 1.1 to 20.5 ng m^{-3}, and the concentration of hopanes

313 was approximately two times of that of steranes. As expected, the total concentrations of hopanes/steranes were 6.7/2.5,

314 3.3/1.2 and 1.9/1.1 ng m^{-3} in petrochemical industry (SH), traffic area (SL) and suburban area (WQ), respectively.

315 The predominant hopane analogs were C_{30}–αβ–H, C_{31}–αβ–S and C_{29}–αβ– NOR–H, with concentrations of 1.2±1.3,

316 0.8±0.7 and 0.8±0.9 ng m^{-3}, respectively. The homohopane index (C_{31}–S/(S+R)) was 0.75, much greater than those of

317 diesel (0.49), gasoline vehicle emissions (0.50–0.62) and petroleum (0.6), but a bit smaller than industrial bitumite coal

318 (0.87) (Fraser et al., 2002). This implies vehicle exhausts, petrochemical emissions and coal combustion have all

319   contributed to particle concentrations. The concentration profiles of steranes were similar at different sites, with ααα–

320   20R–EC being the most abundant, followed by ααα–20R–EC. This pattern was a bit different from that in Delhi which

321   was dominated by C_{29} sterane (Yadav et al., 2013).

3.2 Size-specific distributions

323   Particulate matters within 13 size fractions were collected. The size-specific distribution of NPOCs was then obtained

324   (Fig. 4). The total concentration of PAHs (Fig. 4a) in each size fraction ranged from 0.4 ng m^{-3} in the 0.01–0.018 μm

325   fraction to 5.1 ng m^{-3} in the 0.56–1.00 μm fraction. A bimodal distribution of the concentrations of PAHs was observed,

326   with peaks in 0.56–1.00 and 9.90–18.0 μm fractions, respectively. PAHs in the 0.56–1.00 μm fraction were the most

327   abundant. This phenomenon could be reasonably explained by that heavy molecular weight PAHs tend to be enriched in

328   smaller particles (< 1.4 μm) (Kleeman et al., 2008), whereas light molecular weight PAHs are speculated to adsorbed

329   onto coarse particles by volatilization and condensation. As discussed above, the heavy molecular weight PAHs

330   accounted for 50.6% of the total PAHs in this study. Similarly, Hien et al. (2007) found that PAHs accumulated

331   predominantly in small size fractions (especially < 0.4 μm) in urban aerosols. More recently, Mu et al. (2017) indicated

332   PAHs were strongly correlated with accumulation mode particles (0.05–2.0 μm), and PAHs in this fraction accounted for

333   ~85% of the total measured PAHs. In fact, the relationship between the concentration of PAHs and the size particles is

334   highly variable. This suggests not only source type but also photodegradation and gas-particle partitioning have great

335   influences on the size-specific distribution of PAHs.

336   The concentrations of n-alkanes (Fig. 4b) in Aitken nuclei, Accumulation and Coarse mode particles were 1.7–3.1, 7.0–

337   28.7 and 4.7–6.3 ng m^{-3}, respectively. The concentrations of n-alkanes in individual fractions accounted for 1.5–24.5% of

338   the total measured n-alkanes in all fractions. n-Alkanes in the 0.56–1.00 μm fraction were the most abundant, whereas

339   n-alkanes in three nano-size fractions accounted for the smallest percentages (1.5–2.5%). Notably, the concentration of

340   n-alkanes increased with increase in fraction size. After fraction size reached 1.00 μm, however, the concentration of

341   n-alkanes decreased in coarse mode particles. This implies n-alkanes have a tendency to be adsorbed on fine particles. In

342   general, condensation is more likely happen to fine particles because of their large quantity and larger specific surface

343   area (Wang et al., 2009).

344   The size-specific distribution of hopanes and steranes was illustrated in Fig. 4c. Hopanes and steranes were the most

345   abundant in the following five fractions: 0.56–1.00 μm (2.9 ng m^{-3}), 0.32–0.56 μm (2.5 ng m^{-3}), 0.18–0.32 μm (1.8 ng

346   m^{-3}), 9.9–18 μm (1.2 ng m^{-3}) and 0.10–0.18 μm (1.1 ng m^{-3}). Approximately 55% of ∑(hopanes+steranes) were

347   associated with the 0.10–1.00 μm fraction. This result was consistent with that of Kleeman et al. (2008) who found the

348 hopanes and steranes were abundant in ultrafine size fraction during a severe winter pollution episode in Sacramento,

349 USA.

350
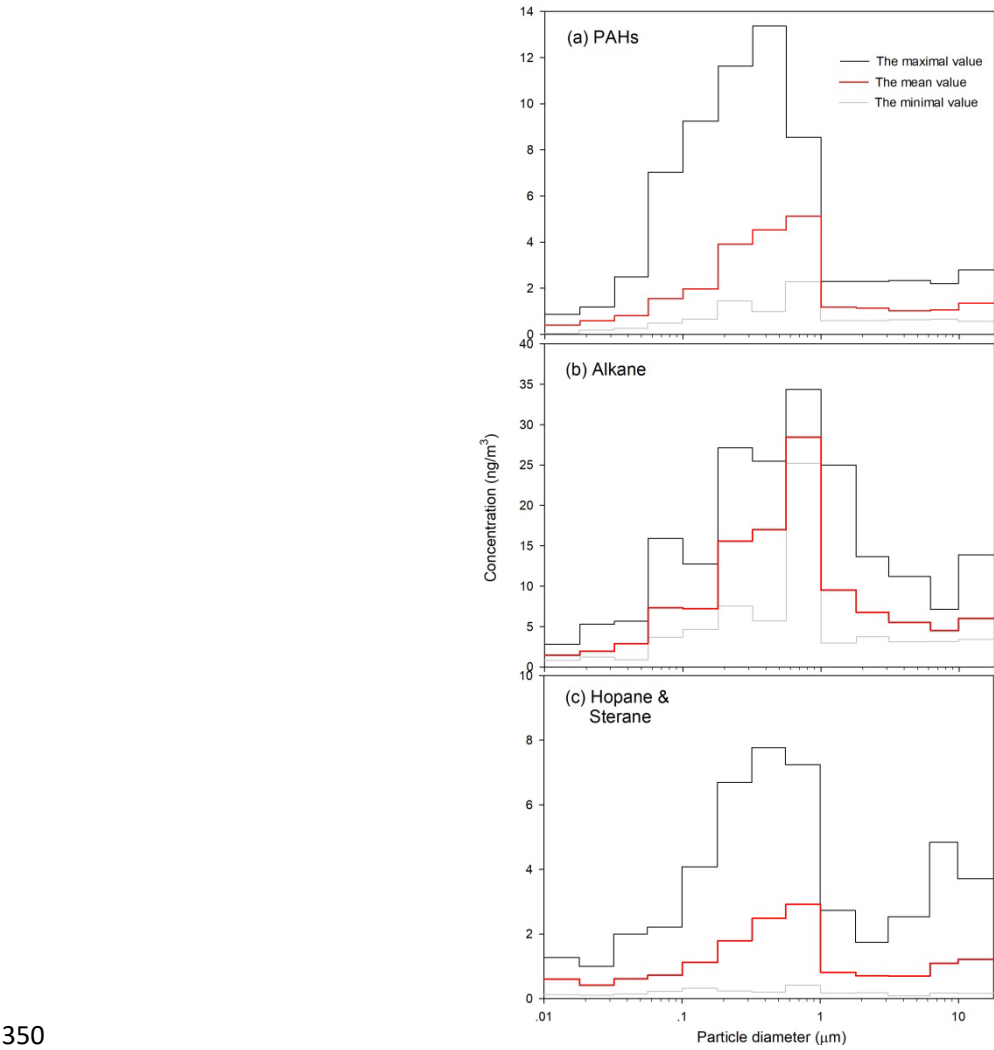
351 **Fig. 4.** Mean-normalized size-specific distribution of NPOCs in the collected PM$_{2.5}$ samples

352 **3.3 Degradation of organics**

353 Photochemical oxidation has great influences on the mass concentration and size-specific distribution of NPOCs, and on

354 their removal and atmospheric fate (May et al., 2012). Ratio–ratio plot was used to visually compare the distributions of

355 critical marker species and investigate their degradation (Robinson et al. 2006;May et al., 2012). Photochemical decay

356 could cause the ambient data to be distributed along a line emanating from the source profile, with increasing

357 photochemical age (Robinson et al., 2006;Yu et al. 2011). The more oxidation, the further ambient ratio is from the

358 source profile. In addition to photochemical decay, the ratio–ratio plot can also be affected by mixed emissions.

359 In this study, IcdP/BghiP and C29–αβ–NOR/C30–αβ–H were adopted to explore the degradation of NPOCs (Robinson et

360 al., 2006;Wang et al., 2016). EC shares common origins with PAHs and hopanes but they are subject to photodegradation.

361 Two pairs of PAHs and hopanes were normalized by EC. The ratio–ratio plot of IcdP and BghiP normalized by EC from

362 different sites was depicted in Fig. 5a, together with vehicle (diesel and gasoline) exhausts, tunnel and coal burning

363 source profiles. Most of the data points were distributed along a line, which overlapped tunnel, vehicle exhaust and

364 industrial coal, implying ambient hopanes in this city were from vehicle emissions and coal combustion. Wang et al.

365 (2016) reported that vehicle emissions contributed to atmospheric hopanes in four cities in PRD. There were several

366 deviation points at left down corner, and the values were smaller than the values of tunnel and vehicle source profile,

367 indicating mixed influence from traffic origins and degradation. Yu et al. (2011) reported a more apparent liner

368 distributions of data sets measured in Hong Kong and PRD, which can be attributed to their single vehicle source type. In

369 Fig. 5b, most of the data were linearly distributed, implying both biomass burning and vehicle emission contribute to

370 hopanes. Robinson et al. (2006) found hopanes were severely depleted in Pittsburgh, USA, and they attributed this

371 phenomenon to regional air mass transport affecting the oxidation of condensed-phase organic compounds.

372
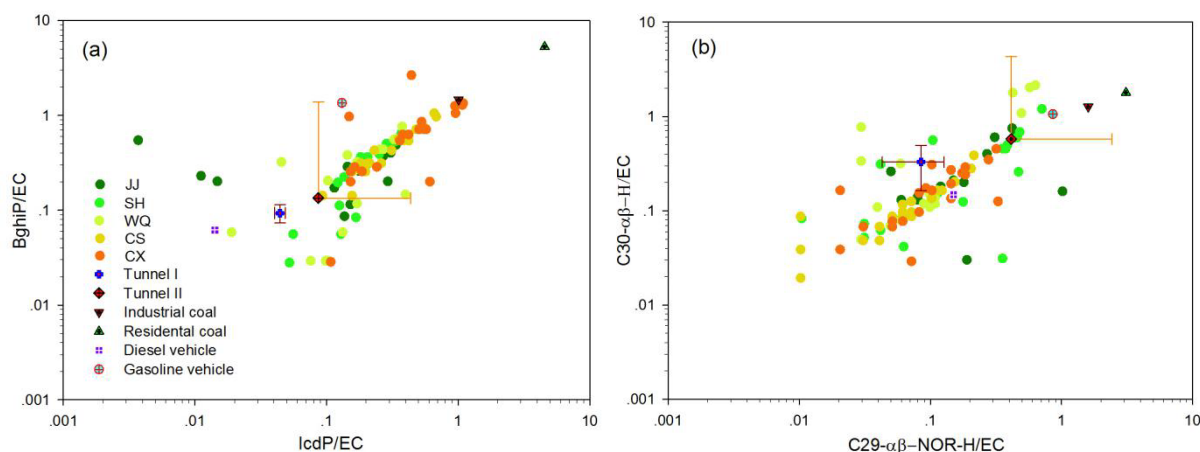
373 **Fig. 5.** Ratio–ratio plots of two pairs of characterized species (IcdP/BghiP and C29–αβ–NOR–H/C30–αβ–H)

374 normalized by EC and published source profiles. (Tunnel I: Yu et al., 2011; Tunnel II: He et al., 2009; Residental

375 coal: Zhang et al., 2008; Industrial coal: Zhang et al., 2008; Diesel vehicle: Fraser et al., 2002; Gasoline vehicle:

376 Fraser et al., 2002)

377 **3.4 Impact of gas-particle partitioning on fine particle source apportionment**

378 **3.4.1 Gas-particle partitioning**

379 An important aspect of atmospheric NPOCs is their gas-particle partitioning behavior, which has effects on their fate and

380 size-specific occurrence. Once NPOCs are emitted into the atmosphere, they subsequently partition between gas and

381 particle phases and a partitioning equilibrium can be reached according to their vapor pressure and temperature

382 dependencies.

383 The particle-phase fraction (φ) of NPOCs was calculated according to the classical gas-particle partitioning model (Fig. 6

384 and Fig. S1). The gas-phase fractions of LMW PAHs (e.g., FLO, PHE, ANT, FLU and PYR) were rather substantial, and

385 their particle-phase fractions (φ) ranged from 2.4% to 51.3%. Similarly, the φ values of short chain C_{22}–C_{24} n-alkanes

386 varied between 21.2% and 62.5%, exhibiting an increasing trend with increase in their molecular weight. However, for

387 the heavier molecular weight species, like PAHs with 5–7 rings, long chain n-alkanes ($> C_{26}$), hopanes and steranes, the φ

388 values remained greater than 90.0% for all temperature ranges. The calculated φ values of PAHs and n-alkanes were

389 comparable to those estimated in urban Denver, Chicago and Los Angeles in USA (Xie et al., 2013), but a bit greater than

390 those in PRD of China (Wang et al., 2016). The lower fractions of NPOCs in gas phase in this study compared with that

391 in PRD was probably because PRD area is located in a border region between subtropics and tropics. This region has

392 higher temperature than Eastern China area, especially in cold winter seasons, and the higher temperature can facilitate

393 the shift of species to gas phase.

394
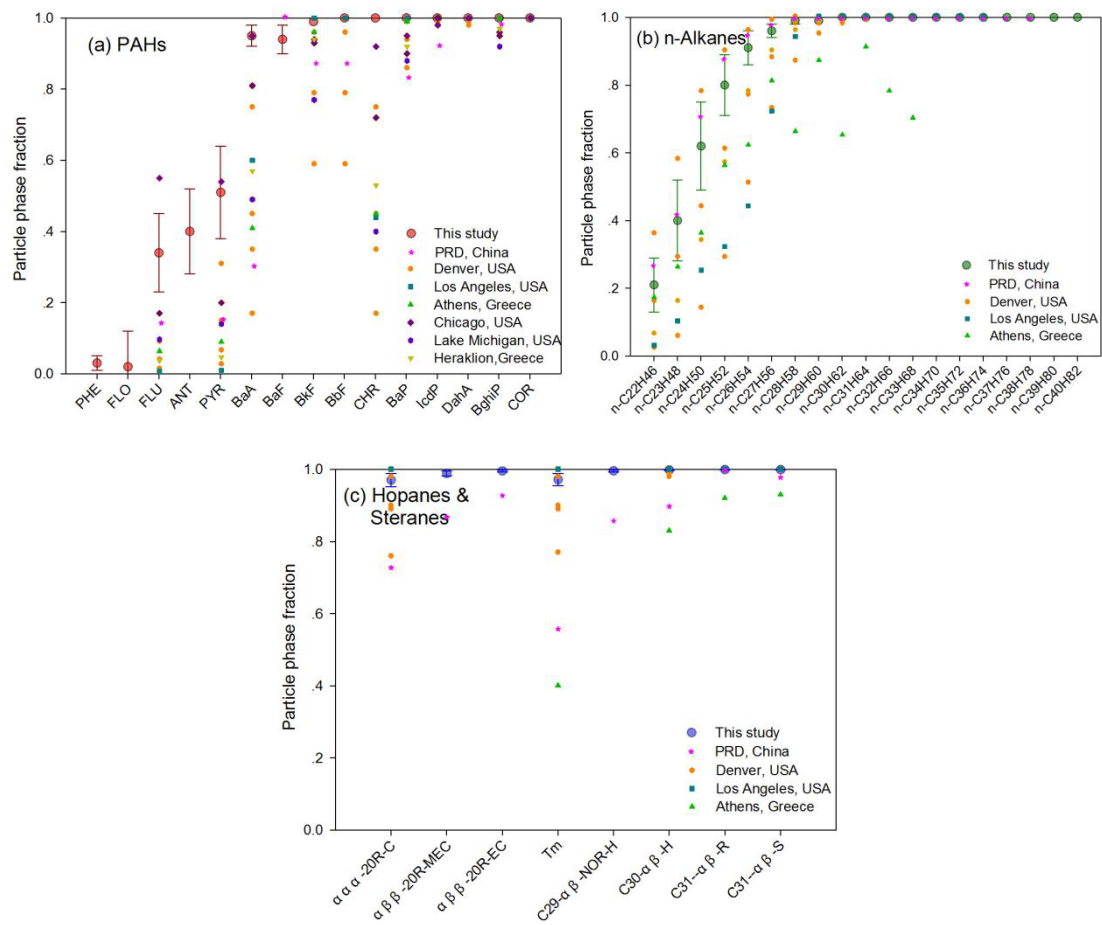
395

396 **Fig. 6.** Average particle-phase fractions (φ) of all NPOCs as in comparison with previous results

397 To further evaluate gas-particle partitioning of NPOCs, φ values were compared with predicted ones by Jungle–Pankow

398 model (Fig. 7). The φ values of LMW PAHs, short chain n-alkanes, $\log P^o_L > -5$ hopanes and steranes, were underpredicted

399 by Jungle–Pankow model. However, the φ values predicted by Jungle–Pankow model agreed well with the calculated

400 ones for HMW PAHs and long chain n-alkanes. Underestimation of φ values of PAHs by Jungle–Pankow model

401 compared with the filed measured ones were also reported by He and Balasubramanian, (2009), and they attributed the

402 discrepancy to the higher OM fractions in real environment than that adopted by the model.
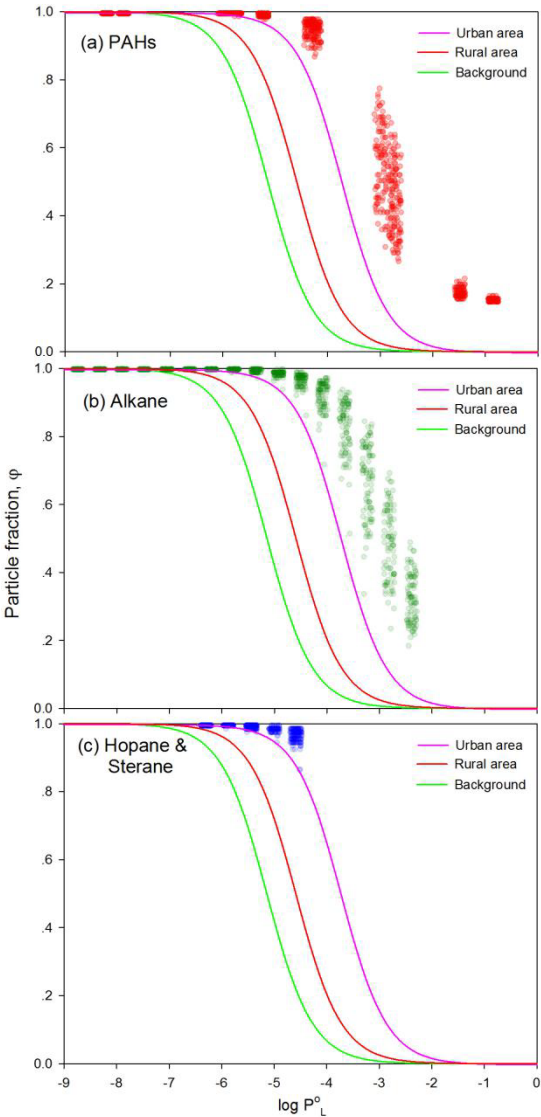
403

404 **Fig. 7.** Comparison of φ values between the measured and predicted results from Jungle–Pankow model

405 **3.4.2 PMF source apportionment**

406 Source apportionment analysis involves techniques that can be used to identify source species and their unique

407 contributions, which are critical in making policies of controlling pollution. It is typically assumed the molecular markers

408 are stable in the ambient environment, *i.e.*, being nonreactive and nonvolatile (May et al., 2012). However, many organic

409 markers can be oxidized over atmospherically relevant time scales, and partition between gas and particle phases. As

410 discussed above, light molecular weight NPOCs tend to shift to gas phase. If the data of NPOCs in single particle phase

411 are directly used as input for receptor model, this may confound the aerosol factors. To explore the impact of gas-particle

412 partitioning on $PM_{2.5}$ source apportionment, the NPOCs in single particle phase and the total NPOCs in gas-particle

413 phases were used as input data for receptor model PMF, respectively.

414 Additionally, chemical constituent of ambient aerosol is an essential step to identifying major sources and quantifying the

415 corresponding contributions to particulate matter. Individual organic tracers, elemental species, inorganic ions and

416 OC/EC have been demonstrated to be able to provide source apportionment of aerosols. Therefore, both input data of

417 single particle phase and the total NPOCs were incorporated with elemental species, inorganic ions and OC/EC. Results

418 based on single particle phase and the total phases were denoted by PMF_P and PMF_T, respectively. Five to eleven factors

419 were extracted in this study to obtain reasonable results. Finally, it turned out that the results of eight factors gave the

420 most reasonable source profiles (Fig. 8 and Fig. S2).

421 Factor 1 (Fig. 8a) was characterized by significant presence of Al, Ca, Mg, Ti and Fe, which are regarded as good

422 indicator of dust (including construction dust, geological dust and road dust) (Wang et al., 2015). These elements are the

423 major elements of dust sand, usually accumulated in the coarse mode particles. Geological dust typically contains high

424 concentrations of crustal elements, including Fe and Mn. Hence, this factor was regard as "dust", with percent

425 contributions of 8.90% and 11.0% under PMF_P and PMF_T, respectively.

426 Factor 2 (Fig. 8b) was characterized by the significant presence of Cu, Mn, Zn, Pb, BkF, BbF, BaF and BaP. Mn, Zn and

427 As are related to emissions from steel production, brick, ceramic and glass making factories (Li et al., 2016;Sulong et al.,

428 2017). Cu mainly originates from non-ferrous metal production and smelting factories. BkF, BbF and BaP are typical

429 markers of emissions from coke industry. Several large-scale industrial parks are located in Jiujiang city, e.g., Shacheng

430 Industry and Jiujiang Comprehensive Industry in the northern and southern areas, respectively. Therefore, factor 2 was

431 associated with industrial emission.

432 Factor 3 (Fig. 8c) was characterized by large fractions of HMW PAHs (IcdP, BghiP, DahA and COR), as well as

433 relatively high fractions of hopanes and steranes. BghiP and COR are excellent tracers of vehicle exhausts. Hopanes and

434 steranes are related to exhausts from heavy-duty vehicles with diesel engines(Wang et al., 2016). As mentioned above,

435 there were over 700 thousand motor vehicles in Jiujiang city in 2015, among which about 1/15 were mainly powered by

436 diesel engines. Therefore, factor 3 was identified as "vehicle related exhausts", with percent contributions of 12.5% and

437 15.0% under PMF_P and PMF_T, respectively.

438 Factor 4 (Fig. 8d) was characterized by the presence of well-documented indicators of secondary aerosol formation, such

439 as NO_3^-, SO_4^{2-} and NH_4^+, with factor fractions of 83.7%, 87.4% and 94.1%, respectively. These secondary products are

440 formed by precursor gases (SO_2 and NOx) via oxidation reactions(Wang et al., 2015). They are mainly emitted from

biomass burning, coal combustion and vehicles. NO_3^-, SO_4^{2-} and NH_4^+ accounted for 19.9–22.3%, 16.4–18.1% and 10.4–13.7% of $PM_{2.5}$ concentrations, respectively, which were typically derived from gas-particle conversion process as well as homogeneous and heterogeneous reactions in urban atmosphere. Furthermore, the similar spatial distribution and contribution in all sites highlight a widespread of these components. Consequently, factor 4 was identified as "secondary aerosol formation".

Factor 5 (Fig. 8e) was characterized by significant presence of C_{30}–C_{40} n–alkanes, as well as relatively significant presence of FLU and PYR. In previous research (Wang et al., 2016), the long chain n–alkanes (C_{29}–C_{36}) were considered to come from local emissions, especially from coal combustion. PYR and FLU are frequently considered as excellent markers of coal combustion for aerosol source apportionment. Coal is the primary energy source for many industries in China. About 3.1 million tons of standard coal are consumed per year by the Jiujiang thermal power plant according to local statistics. Thus, factor 5 was identified as "coal burning", with percent contributions of 18.7% and 16.4% under PMF_P and PMF_T, respectively.

Factor 6 (Fig. 8f) was characterized by high percentage of Cl^- and K^+, with some amounts of As, Se, Pb, OC and EC. Cl^- and K^+ have been widely used as tracers of wood and biomass burning aerosol (Li et al., 2016). In the past, crop straws were disposed bu local farmers in the field by burning for convenience. Although this has been extensively banned in recent years, several large-scale straw burning sites surrounding this city can still be observed by China National Satellite Meteorological Center (http://hjj.mep.gov.cn/jgjs/). Thus, this factor was considered as "biomass burning", with percent contributions of 12.7% and 15.7% under PMF_P and PMF_T, respectively.

Factor 7 (Fig. 8g) was characterized by high fraction of Ni and V, which are excellent tracers of exhausts from ship and heavy-duty diesel vehicles. In fact, Jiujiang harbor is among the ten busiest harbors in Yangtze River, whose port cargo throughput is 59 million tons per year. Hence, factor 7 was identified as "shipping and diesel exhausts".

Factor 8 (Fig. 8h) was characterized by a high load of short chain n–alkanes ($C_{22}H_{46}$, 76.6%; $C_{23}H_{48}$, 84.2%; $C_{24}H_{50}$, 81.1%) and LMW PAHs (about 60% for FLU, PYR, BaA and CHR). These species have several characteristics: most of their particle-phase fractions (φ) were less than 50%; relatively light molecular weight; strongly temperature-dependent vaporization. These compounds have been interpreted as "light NPOCs factor" in previous research (Xie et al., 2013;Wang et al., 2016). The percent contributions of this factor were 3.7% and 5.6% under PMF_P and PMF_T, respectively. Additionally, concentrations of light NPOCs factor showed an increasing trend with increase in temperature, implying the association of this factor with fossil fuel evaporation and biogenic emissions. Hence, this factor was regarded as "light NPOCs factor".

Fig. 8. Source profiles of eight sources resolved by PMF

470
471

3.4.3 Assessing impacts of gas-particle partitioning on source apportionment

As stated above, using the data of single particle phase as input data for PMF model could lead to uncertainty in results, which was related to gas-particle partitioning of NPOCs in the mathematical solution. In the present study, the eight extracted factors in this study showed similar source profiles between PMF_P and PMF_T. This phenomenon could reasonably occur because of the major NPOCs compounds were enriched in particle phase in the present study, meanwhile, the concentrations of hopanes and steranes in gas phase were relatively low. In sharp contrast with this study, Wang et al. (2016) extracted an extra light NPOCs factor in PMF_P in PRD, and they found very volatile NPOCs (like FLU) were quite variable in PMF_T, but almost did not appear in PMF_P. This difference could probably be due to the $PM_{2.5}$ source identification in this study was focused on the period of high-frequency haze episodes (late autumn and winter), while the research conducted in PRD included hot summer season which enhanced the uncertainty and variability of predicted light NPOCs.

Gas-particle partitioning has important effect on the occurrence, atmospheric lifetime and transformation of NPOCs. Also, size-specific aerosol distribution and photochemical oxidization have influence on gas-particle partitioning. For example, gas phase oxidation reaction is much faster than heterogeneous reactions, since the uptake of heterogeneous oxidant is diffusion-limited. The empirical and model predicted particle concentrations would be underestimated or overestimated, compared with filed measured values. It may add the uncertainty for the input data of receptor model. In this study, using the data of total organic compounds in gas-particle phases with other aerosol species as input data for receptor model provides an excellent tool for $PM_{2.5}$ source apportionment. However, reasonable caution should still be given to the more volatile organic species.

4. Conclusions

NPOCs are typical molecular markers for source identification, which attract researchers' interest worldwide. To the best of our knowledge, this is the first research analyzing size-specific aerosols-associated NPOCs, conducted in a typical middle-scale city in Eastern China. Fifty-seven $PM_{2.5}$-associated NPOCs including PAHs, n–alkanes, iso–alkanes, hopanes and steranes were identified and quantified using a TD–GC/MS method. The total concentrations of NPOCs were 31.7–388.7 ng m^{-3}, with n-alkanes being the most abundant species (67.2%). The heavy molecular weight PAHs (4- and 5-ring) contributed 67.9% of the total PAHs, and the middle chain length (C_{25}–C_{34}) n-alkanes were the most abundant in n-alkanes. The MDRs showed that 83.0% of NPOCs were originated from anthropogenic sources, including pyrogenic source, fossil fuel combustion and biomass burning.

PAHs and n-alkanes were majorly enriched in 0.56–1.00 μm fraction, and ∑(hopanes+steranes) were associated with 0.32–1.00 μm fraction. The nano-size and coarse mode particles showed low concentrations of NPOCs. The ratio–ratio plots of IcdP/BghiP and C29–αβ–NOR/C30–αβ–H normalized by EC implied that NPOCs in local area were affected by photochemical degradation and emissions from mixed sources. Gas-particle partitioning model showed that the calculated particle-phase fraction (φ) of the light molecular weight NPOCs ranged between 2.4% to 62.5%, while those of heavy PAHs, long chain n-alkanes, hopanes and steranes were high (>90.0%). Using data based on single particle phase and on gas-particle phases with other $PM_{2.5}$ compounds as input data for PMF model, respectively, we successfully extracted eight factors from both cases. The PMF_T (the case of gas-particle phases) showed better source profiles than PMF_P (the case of single particle phase), and the light NPOCs factor contributed a bit more in PMF_T (5.6%) than in PMF_P (3.7%). This study indicates that NPOCs are useful for aerosol apportionment, and total NPOCs in two phases enable better source profiles than NPOCs in single particle phase.

Acknowledgement

This study was financially supported by National Natural Science Foundation of China (No. 21577090 and No.21777094) and Jiujiang Committee of Science and Technology (Grant No. JXTCJJ2016130099). We thank Jiujiang Environmental Protection Agency and Jiujiang Environmental Monitor Station for coordinating the sampling process and for their valuable contribution to field measurement. We appreciate senior engineer Yajuan Zhou (Instrumental Analysis Center, Shanghai Jiao Tong University) for her assistance in experimental analysis.

References

And, J. S. C., and Hanshaw, W.: Vapor Pressures and Vaporization Enthalpies of the n-Alkanes from C31 to C38 at T = 298.15 K by Correlation Gas Chromatography, J. Chem. Engineering Data, 49, págs. 620-630, 2004.

Chen, P., Li, C., Kang, S., Rupakheti, M., Panday, A. K., and Zhang, Q.: Polycyclic aromatic hydrocarbons (PAHs) in aerosols over the central Himalayas along two south-north transects, Atmos. Chem. Phys., 18, 1-38, 2016a.

Chen, X., Balasubramanian, R., Zhu, Q., Behera, S. N., Bo, D., Huang, X., Xie, H., and Cheng, J.: Characteristics of atmospheric particulate mercury in size-fractionated particles during haze days in Shanghai, Atmos. Environ., 131, 400-408, 2016b.

Ding, L. C., Ke, F., Wang, D. K. W., Dann, T., and Austin, C. C.: A new direct thermal desorption-GC/MS method: Organic speciation of ambient particulate matter collected in Golden, BC, Atmos. Environ., 43, 4894-4902, 2009.

527   Feng, J., Hu, M., Chan, C. K., Lau, P. S., Fang, M., He, L., and Tang, X.: A comparative study of the organic matter in

528   PM2.5 from three Chinese megacities in three different climatic zones, Atmos. Environ., 40, 3983-3994, 2006.

529   Fraser, M. P., Lakshmanan, K., Fritz, S. G., and Ubanwa, B.: Variation in composition of fine particulate emissions from

530   heavy-duty diesel vehicles, J. Geophys. Res. Atmos., 107, ICC 8-1-ICC 8-6, 2002.

531   Hao, Y., and Liu, Y. M.: The influential factors of urban PM 2.5 concentrations in China: aspatial econometric analysis, J.

532   Cleaner Production, 112, 1443-1453, 2015.

533   He, J., and Balasubramanian, R.: A study of gas/particle partitioning of SVOCs in the tropical atmosphere of Southeast

534   Asia, Atmos. Environ., 43, 4424-4434, 2009.

535   Hien, T. T., Le, T. T., Kameda, T., Takenaka, N., and Bandow, H.: Distribution characteristics of polycyclic aromatic

536   hydrocarbons with particle size in urban aerosols at the roadside in Ho Chi Minh City, Vietnam, Atmos. Environ., 41,

537   1575-1586, 2007.

538   Ho, S. S., and Yu, J. Z.: In-injection port thermal desorption and subsequent gas chromatography-mass spectrometric

539   analysis of polycyclic aromatic hydrocarbons and n-alkanes in atmospheric aerosol samples, J. Chromatography A, 1059,

540   121, 2004.

541   Ho, S. S. H., Yu, J. Z., Chow, J. C., Zielinska, B., Watson, J. G., Sit, E. H. L., and Schauer, J. J.: Evaluation of an

542   in-injection port thermal desorption-gas chromatography/mass spectrometry method for analysis of non-polar organic

543   compounds in ambient aerosol samples, J. Chromatography A, 1200, 217-227, 2008.

544   He, L. Y., Hu, M., Zhang, Y. H., Huang, X. F., Yao, T. T.: Fine particle emissions from on-road vehicles in the Zhujiang

545   tunnel, China. Environ. Sci. Technol., 42(12), 4461-4466, 2008.

546   Huang, R. J., Zhang, Y., Bozzetti, C., Ho, K. F., Cao, J. J., Han, Y., Daellenbach, K. R., Slowik, J. G., Platt, S. M., and

547   Canonaco, F.: High secondary aerosol contribution to particulate pollution during haze events in China, Nature, 514, 218,

548   2014.

549   Huang, X., Liu, Z., Liu, J., Hu, B., Wen, T., Tang, G., Zhang, J., Wu, F., Ji, D., and Wang, L.: Chemical characterization

550   and synergetic source apportionment of PM2.5 at multiple sites in the Beijing–Tianjin–Hebei region, China, Atmos.

551   Chem. Phys.,1-34, 2017.

552   Kim, D. G., Choi, K. I., and Lee, D. H.: Gas-particle partitioning and behavior of dioxin-like PCBs in the urban

553   atmosphere of Gyeonggi-do, South Korea, Atmos.Res., 101, 386-395, 2011.

554   Kleeman, M. J., Riddle, S. G., and Jakober, C. A.: Size distribution of particle-phase molecular markers during a severe

555   winter pollution episode, Environ. Sci. Technol., 42, 6469-6475, 2008.

556   Kuang, Y. W., Huang, Z. H., Wen, D. Z., Li, J., and Huang, L. B.: Unravelling airborne polycyclic aromatic hydrocarbons

(PAHs) in southern China using tree-rings of 100-yr old Pinus Kwangtungensis, Atmos. Chem. Phys. Discussions, 11, 27359-27382, 2011.

Li, J., Wang, G., Ren, Y., Wang, J., Wu, C., Han, Y., Zhang, L., Cheng, C., and Meng, J.: Identification of chemical compositions and sources of atmospheric aerosols in Xi'an, inland China during two types of haze events, Sci. Total Environ., 566-567, 230, 2016.

Li, L., Tan, Q., Zhang, Y., Feng, M., Qu, Y., An, J., and Liu, X.: Characteristics and source apportionment of PM2.5 during persistent extreme haze events in Chengdu, southwest China, Environ. Pollution, 230, 718, 2017.

Li, Y. C., Yu, J. Z., Ho, S., Schauer, J. J., Yuan, Z. B., Lau, A. K. H., and Louie, P. K. K.: Chemical characteristics and source apportionment of fine particulate organic carbon in Hong Kong during high particulate matter episodes in winter 2003, Atmos. Res., 120–121, 88-98, 2013.

Ma, W. L., Sun, D. Z., Shen, W. G., Yang, M., Qi, H., Liu, L. Y., Shen, J. M., and Li, Y. F.: Atmospheric concentrations, sources and gas-particle partitioning of PAHs in Beijing after the 29th Olympic Games, Environ. Pollution, 159, 1794-1801, 2011.

Ma Y., Dai H., Li L., Chen C., Sun Q, Fan J., Li Y., Huang T.: A rapid method for screening on organic pollutants in PM$_{2.5}$ using GCMS combined with compound composer software, Environ. Chem. 37(1), 188-191, 2018.

May, A. A., Saleh, R., Hennigan, C. J., Donahue, N. M., and Robinson, A. L.: Volatility of organic molecular markers used for source apportionment analysis: measurements and implications for atmospheric lifetime, Environ. Sci. Technol., 46, 12435, 2012.

Mu, L., Peng, L., Liu, X., He Q., Bai, H., Yan,Y., Li Y.: Emission characteristics and size distribution of polycyclic aromatic hydrocarbons from coke production in China, Atmos. Res., 197, 113-120, 2017.

Okonski, K., Degrendele, C., Melymuk, L., Landlová, L., Kukučka, P., Vojta, Š., Kohoutek, J., Čupr, P., and Klánová, J.: Particle Size Distribution of Halogenated Flame Retardants and Implications for Atmospheric Deposition and Transport, Environ. Sci. Technol., 48, 14426-14434, 2014.

Pankow, J. F.: An absorption model of the gas/aerosol partitioning involved in the formation of secondary organic compounds, Atmos. Environ., 28, 189-193, 1994.

Rajput, P., and Sarin, M. M.: Polar and non-polar organic aerosols from large-scale agricultural-waste burning emissions in Northern India: Implications to organic mass-to-organic carbon ratio, Chemosphere, 103, 74-79, 2014.

Robinson, A. L., Donahue, N. M., and Rogge, W. F.: Photochemical oxidation and changes in molecular composition of organic aerosol in the regional context, J. Geophy. Res. Atmos., 111, 375-402, 2006.

Rogge W F, Hildemann L M, Mazurek M A.: Sources of fine organic aerosol. 6. Cigaret smoke in the urban atmosphere.

587   Environ. Sci. Technol., 28(7):1375-88, 1994.

588   Shen, X. J., Sun, J. Y., Zhang, X. Y., Zhang, Y. M., Zhang, L., Che, H. C., Ma, Q. L., Yu, X. M., Yue, Y., and Zhang, Y. W.:

589   Characterization of submicron aerosols and effect on visibility during a severe haze-fog episode in Yangtze River Delta,

590   China, Atmos. Environ., 120, 307-316, 2015.

591   Sulong, N. A., Latif, M. T., Khan, M. F., Amil, N., Ashfold, M. J., Mia, W., Chan, K. M., and Sahani, M.: Source

592   apportionment and health risk assessment among specific age groups during haze and non-haze episodes in Kuala

593   Lumpur, Malaysia, Sci. Total Environ., 601–602, 556-570, 2017.

594   Wang, G., Kawamura, K., Xie, M., and Hu, S.: Size-distributions of n-hydrocarbons, PAHs and hopanes and their sources

595   in the urban, mountain and marine atmospheres over East Asia, Atmos. Chemi. Phys. Discussions, 9, 8869-8882, 2009.

596   Wang, G., Kawamura, K., Xie, M., Hu, S., Gao, S., Cao, J., An, Z., Wang, Z.: Size-distributions of n-alkanes, PAHs and

597   hopanes and their sources in the urban, mountain and marine atmospheres over East Asia. Atmos. Chem. Phy. 9,

598   8869-8882, 2009.

599   Wang, Q., Zhuang, G., Huang, K., Liu, T., Deng, C., Xu, J., Lin, Y., Guo, Z., Chen, Y., and Fu, Q.: Probing the severe

600   haze pollution in three typical regions of China: Characteristics, sources and regional impacts, Atmos. Environ., 120,

601   76-88, 2015.

602   Wang, Q., Feng, Y., Huang, X. H. H., Griffith, S. M., Zhang, T., Zhang, Q., Wu, D., and Yu, J. Z.: Non-polar organic

603   compounds as PM2.5 source tracers: Investigation of their sources and degradation in the Pearl River Delta, China, J.

604   Geophy. Res. Atmos, 2016.

605   Xie, M., Barsanti, K. C., Hannigan, M. P., Dutton, S. J., and Vedal, S.: Positive matrix factorization of PM2.5 -

606   eliminating the effects of gas/particle partitioning of semivolatile organic compounds, Atmos. Chemi. Phys., 13, 7381,

607   2013.

608   Xie, M., Hannigan, M.P., Barsanti, K.C.: Impact of Gas/Particle Partitioning of Semivolatile Organic Compounds on

609   Source Apportionment with Positive Matrix Factorization. Environ. Sci. Technol. 48, 9053-9060, 2014.

610   Xie, Y., Ye, X., Ma, Z., Tao, Y., Wang, R., Zhang, C., Yang, X., Chen, J., and Chen, H.: Insight into winter haze formation

611   mechanisms based on aerosol hygroscopicity and effective density measurements, Atmos. Chemi. Phys., 17, 7277-7290,

612   2017.

613   Xu, H. M., Tao, J., Ho, S. S. H., Ho, K. F., Cao, J. J., Li, N., Chow, J. C., Wang, G. H., Han, Y. M., and Zhang, R. J.:

614   Characteristics of fine particulate non-polar organic compounds in Guangzhou during the 16th Asian Games:

615   Effectiveness of air pollution controls, Atmos. Environ., 76, 94-101, 2013.

616   Yadav, S., Tandon, A., and Attri, A. K.: Characterization of aerosol associated non-polar organic compounds using

TD-GC-MS: a four year study from Delhi, India, J. Hazard. Materials, 252–253, 29-44, 2013.

Yu, J. Z., Huang, X. H., Ho, S. S., and Bian, Q.: Nonpolar organic compounds in fine particles: quantification by thermal desorption-GC/MS and evidence for their significant oxidation in ambient aerosols in Hong Kong, Analytical Bioanalytical Chem., 401, 3125-3139, 2011.

Zhang, Y. L., Huang, R. J., El Haddad, I., Ho, K. F., Cao, J. J., Han, Y., Zotter, P., Bozzetti, C., Daellenbach, K. R., and Canonaco, F.: Fossil vs. non-fossil sources of fine carbonaceous aerosols in four Chinese cities during the extreme winter haze episode of 2013, Atmos. Chemi. Phys., 15, 1299-1312, 2015.

Zhao, Y., Zhang, Y., Fu, P., Ho, S. S., Ho, K. F., Liu, F., Zou, S., Wang, S., and Lai, S.: Non-polar organic compounds in marine aerosols over the northern South China Sea: Influence of continental outflow, Chemosphere, 153, 332, 2016.